Processing Characteristics and Structure Development in Solid-State Extrusion of a New Semicrystalline Polyimide (BTDA–DMDA)

Y. D. WANG,[1] M. CAKMAK,[1,*] and F. W. HARRIS[2]

[1]Institute of Polymer Engineering and [2]Institute of Polymer Science, College of Polymer Engineering and Polymer Science, University of Akron, Akron, Ohio 44325-0301

SYNOPSIS

In this article, we present detailed processing characteristics and structure development in a thermoplastic polyimide BTDA–DMDA in the solid-state extrusion process. This fully imidized polyimide polymer is known to crosslink at fast rates when it is brought to a molten phase even for short periods of time. This characteristic makes it difficult to process it in the molten phase and attempts at melt processing result in melt fracture and highly distorted extrudates. However, this polymer can be shaped into high-quality extrudates when it is processed below its melting temperature directly from its postpolymerization powdered state. The solid-state extrusion of precompacted BTDA–DMDA powder was studied in the temperature range from 250 to 320°C. At the temperatures from 290 to 320°C, high-quality extrudates were obtained. Below 290°C, solid-state extrusion was not possible due to the limitation of the load cell capacity of the capillary rheometer used in this research. Above 320°C, the extrudates were found to be of poor quality as a result of degradation and crosslinking in the molten phase. Structural characteristics of the samples produced by solid-state extrusion was investigated by the microbeam X-ray diffraction technique. The thermal behavior of the extrudates was also characterized by differential scanning calorimetry (DSC). The DSC results show that at low extrusion temperatures the samples exhibit dual endothermic peaks and are highly crystalline in an extruded state. The higher melting peak located at about 350°C is due to the melting of the new crystalline phase that has developed partially during the solid-state extrusion process and partially during the recrystallization process that takes place at temperatures at and slightly above the primary melting process during the DSC heating scan. This has been confirmed by DSC, depolarized light hot-stage video microscopy, and wide-angle X-ray diffraction studies. The long spacing of the higher melting crystals was found to be much larger than that of the lower melting crystals, as evidenced by the small angle X-ray scattering studies.

INTRODUCTION

BTDA–DMDA was synthesized with the aim of developing new impact/solvent resistant resins for various aerospace applications.[1,2] However, it was found that the melt extrusion of this polymer is not possible at temperatures where it is partially or completely molten as a result of degradation and crosslinking. The technique of solid-state extrusion has a long history[3–14] and has been successfully applied to both noncrystallizable as well as crystallizable polymers to obtain high-modulus and high-strength parts by subjecting them to deformation below their typical melt-processing temperatures. The temperatures between the crystalline relaxation temperature (sometimes designated as the α-transition) and melting temperatures were found to be suitable for semicrystalline polymers. With solid-state extrusion, not only the mechanical properties of the polymers are improved but also the optical

* To whom correspondence should be addressed.

Journal of Applied Polymer Science, Vol. 56, 837–851 (1995)
 CCC 0021-8995/95/070837-15

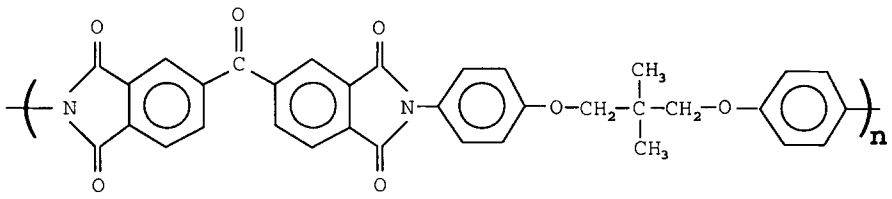

Figure 1 BTDA–DMDA chemical structure.

properties. The solid-state extruded parts from semicrystalline polymers generally exhibit high optical clarity due to reduction in the crystallite sizes to below the wavelength of visible light, thereby reducing the scattering effects.[15] Sometimes, the polymer to be solid-state-extruded is sandwiched between two sacrificing layers of another polymer (e.g., HDPE) and extruded to obtain a high-quality surface finish.[16-18] Some of the polymers that have been successfully solid-state-extruded include polyethyleneterephthalate (PET),[16] poly(ethylene oxide) (PEO)/poly(methyl methacrylate) (PMMA) blends,[17] PP,[19-24] PE,[22,25,26] PVF_2,[22] poly(4-methyl pentene-1) (P4MP1),[27] poly(ethylene-chlorotrifluoro-ethylene),[28] PTFE,[29] nylon 6,6,[12,30] POM,[30] and polycarbonate (PC).[31] Aharoni and Sibilia[32] reviewed the literature on the solid-state extrudability of semicrystalline polymers up to 1979. Southern et al. also published a review article more recently on the solid-state extrusion of polymers.[33]

Because of the above-mentioned difficulties experienced in the melt processing of BTDA–DMDA, we undertook detailed studies to obtain optimum solid-state processing conditions and resulting structural characteristics in the extruded parts.

EXPERIMENTAL

Materials

The BTDA–DMDA with the chemical structure shown in Figure 1 was synthesized from 3,3',4,4'-benzophenonetetracarboxylic dianhydride (BTDA) and 2,2-dimethyl-1,3-(4-aminophenoxy)propane (DMDA) to a low molecular weight level (molecular weight M_n = 10,000). The detailed polymerization procedures can be found in Refs. 1 and 2. As-received BTDA–DMDA powders were vacuum-dried at 100°C for 48 h to remove the moisture. The dried powders were then subjected to the solid-state extrusion and compression-molding processes immediately after drying.

Solid-State Extrusion

A table-top Instron capillary rheometer was used to extrude the samples. This instrument is equipped with a 5000 lb_f (22,240 N) compression load cell and 0.9525 cm-diameter barrel. Three special extrusion dies were designed and built in our laboratories.[34] The geometry of these dies is shown in Figure 2. A special adapter was designed and built to mount these dies on the rheometer.

First, the powders were precompacted at 230°C with a force of 3000 lb_f (13,344 N) with the exit of the die plugged with a special plug. This lower compacting temperature was necessary to remove the entrapped bubbles and to minimize processing problems at elevated extrusion temperatures. After the compaction, the barrel was then heated to the

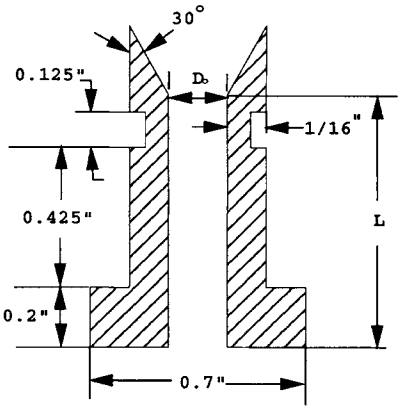

Die	Diameter Do	L	Area reduction ratio
D1	4.80 mm	22.9 mm	3.94
D2	3.34 mm	20.3 mm	8.13
D3	1.41 mm	20.3 mm	45.63

Figure 2 Solid-state extrusion capillary geometry and dimensions.

desired extrusion temperature in about 20 min. During this heating process, pressure was maintained on the compacted mass. To determine the optimum processing window, the solid-state extrusion was first performed at temperatures from 250 to 360°C using the largest diameter die at a crosshead speed of 25.4 mm/min. These experiments were then repeated at temperatures from 290 to 330°C at 5°C intervals using a 0.381 mm/min crosshead speed for the other two dies of varying L/D ratios which provided different levels of deformation in the extrudate. The lower-temperature side of the processing window was limited by the load-cell capacity of the rheometer. Once this limit was reached, the process was stopped. After the extrudates equilibrated at room temperature for at least 1 week, the extrudate swell was measured.

Thermal Characterization

DSC thermal analysis of the BTDA–DMDA extrudates were performed using a DuPont DSC 910 apparatus. The samples of approximately 10 mg were crimped in the DSC pans and scanned at a 20°C/min heating rate in a dry nitrogen atmosphere. To verify the origin of the higher melting peak, a series of DSC scans were also performed with heating rates of 5, 20, and 50°C/min on selected samples.

To study the structural gradient development in the solid-state extruded parts, the cutting procedure shown in Figure 3 was used to obtain samples at different radial locations in the extrudate produced with the largest die (Do = 4.80 mm) at 310°C using a 25.4 mm/min crosshead speed. These samples were analyzed using the DuPont DSC 910 as described above.

The decomposition temperatures of the BTDA–DMDA powder in air and in a dry nitrogen atmosphere were determined using a DuPont 951 thermogravimetric analyzer at a constant heating rate of 10°C/min. The sample sizes were kept at approximately 5 mg.

Hot-Stage Polarized Video Microscopy

To identify the multiple endothermic peaks observed in the DSC scans, a Linkam hot stage (THM 600) was used to monitor the melting sequence of the BTDA–DMDA extrudate obtained at 310°C using 4.8 mm-diameter capillary. The hot stage was placed on an optical microscope (LEITZ LABORLUX 12 POL S). The heating scan was performed from 30 to 400°C at a heating rate of 5°C/min. The whole melting sequence was recorded on a video cassette

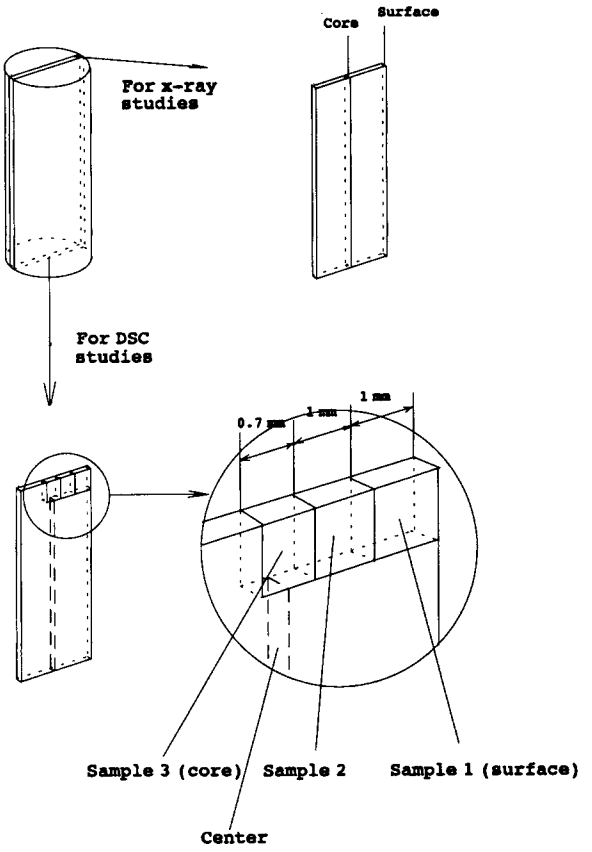

Figure 3 Sample cutting procedures for DSC and WAXD studies.

through which the optical images at different temperatures were later captured and converted to 8 bit gray scale images using an image analysis system. The transmitted light intensity averaged over a large area at each temperature was then obtained using image analysis software. Since the experiment was performed under a cross-polarized light condition, the transmitted light intensity is a depolarized light intensity and roughly proportional to the crystallinity of the sample. By tracing the transmitted light intensity as a function of temperature, one can monitor the crystallization and melting processes that take place at different temperatures.

Matrixing Microbeam Wide-Angle X-ray Diffraction

To study the orientation gradient developed during solid-state extrusion, the sample obtained using the largest die (Do = 4.80 mm) at 310°C with a crosshead speed of 25.4 mm/min was sectioned as shown in Figure 3. The wide-angle X-ray diffraction (WAXD) patterns were obtained at a series of locations from

surface to core of the extrudate using a matrixing microbeam camera equipped with precision x–y translation stages. This camera was mounted on a 12 kW Rigaku rotating anode generator and a nickel foil filter was used to obtain the CuKα radiation. The X-ray beam size was 100 μm.

To evaluate the effect of temperature on the average orientation development, the extrudates produced at different temperatures using the smallest die (Do = 1.41 mm) were also analyzed using the microbeam X-ray diffraction technique. In this series of experiments, the whole extrudate was mounted on the sample holder and the X-ray beam was focused on the cylindrical extrudate in such a way that it passed through the symmetry axis of the sample.

WAXS diffractometer profiles on the BTDA–DMDA extrudates and the compression-molded film were obtained using a Rigaku Rotaflex 12 kW rotating copper anode X-ray generator which was operated at 40 kV and 150 mA. The X-rays were monochromated with a graphite monochromator located between the sample and the detector.

Small-Angle X-ray Scattering

Small-angle X-ray scattering (SAXS) patterns on selected samples were obtained on a GE X-ray generator equipped with a Furnas X-ray camera. A nickel foil filter was used to obtain the CuKα radiation and vacuum was applied to the camera to reduce the air scattering. The sample-to-film distance was 50.25 cm.

RESULTS AND DISCUSSION

Solid-State Extrusion and Thermal Behavior of BTDA–DMDA

To determine the optimum processing temperature and to evaluate the thermal behavior of the as-received material, we performed a DSC scan on the initial BTDA–DMDA powder at a heating rate of 20°C/min. As shown in Figure 4, the glass transition temperature of the initial BTDA–DMDA powder is about 190°C and the polymer undergoes cold crystallization during the scan as indicated by the exothermic peak around 210–250°C. The melting process spans a quite wide range from 280 to 340°C. Above the primary endothermic peak, an additional smaller peak is observed around the 340–370°C range. The area under the cold crystallization peak in the first run is much smaller than that of the

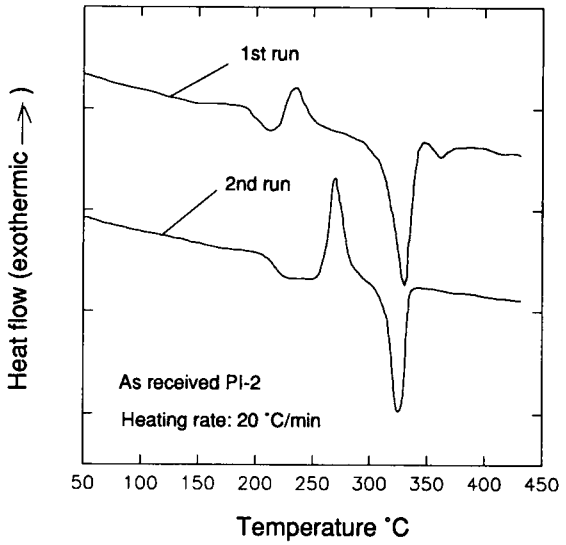

Figure 4 DSC thermograms of initial BTDA–DMDA.

melting peak, indicating that the initial BTDA–DMDA is crystalline. To further investigate the thermal behavior of this material, a second scan of the same sample was performed after cooling it from 430°C to room temperature at a cooling rate of approximately 50°C/min. As shown in Figure 4, the glass transition temperature shifts from 190°C (first scan) to 207°C (second scan), possibly as a result of crosslinking, and the cold crystallization temperature shifts to higher temperature (268°C) in the second scan. The higher endothermic peak at about 360°C observed in the first scan disappears in the second scan. In the second scan, the melting peak shifts to a lower temperature, 322°C, and the area under the cold crystallization peak is about the same as is the area under the melting peak, indicating that, after the first scan, the material remains amorphous due to the fast quenching process. This thermal behavior is typical of aromatic polymers with slow crystallization behavior such as PET, PPS, and PEEK and many process technologies to form highly oriented films take advantage of such behavior. In such processes, the deformation is applied in the region between the glass transition temperature and the cold crystallization temperature where the material behaves in a rather rubbery manner and subsequently annealed as in the tentering frame film process. However, in this polymer, this processing window is rather narrow in the as-received material. There is virtually no temperature gap between the T_g and T_{cc} and thermally activated crystallization starts to occur immediately above the glass transition temperature. Our attempts to extrude in this narrow temperature region were not

successful partly because of the limitation of the load cell in the extrusion instrument. This is caused by rapid thermal crystallization of the sample at this temperature.

The TGA experiments are rather useful in mapping the useful processing window. Figure 5 shows the TGA curves obtained in air as well as in dry nitrogen. Although there appears a slight weight loss at around 300°C, the polymer does not start to lose a significant amount of weight until around 429°C (5% weight loss) in air and 456°C in an nitrogen atmosphere. As far as the volatile byproducts are concerned, the polymer appears to be stable up to about 400°C. We then decided to limit our research activities to a maximum temperature of 360°C. However, the BTDA–DMDA material was found to be very difficult to extrude at temperatures above its melting region. As shown in Figure 6, the extrudates obtained at 335, 350, and 360°C and at a crosshead speed of 25.4 mm/min (Do = 4.80 mm) showed melt fracture phenomena and the color of the extrudates becomes dark as the extrusion temperature increases, indicating that the material has degraded. As the extrusion temperature is decreased, the quality of extrudates increases dramatically and surfaces of the extrudates become smooth (see sample extruded at 310°C).

The extrusion process was repeated for the other two dies with smaller diameters at temperatures ranging from 250 to 330°C and at the crosshead speed of 0.381 mm/min. Due to the load cell limitations, we were not able to extrude the BTDA–DMDA below 313°C for the smallest diameter die (Do = 1.41 mm) and 305°C for the medium diameter die (Do = 3.34 mm). This, however, is merely the limitation of the specific instrument used in this research and solid-state extrusion of the BTDA–DMDA sample should be possible at lower temperatures with higher load capacity instruments. Figure 7 and 8 show the pictures of the extrudates obtained at different temperatures using these two smaller diameter dies. The basic behavior is similar to that obtained for the largest diameter die. As the temperature of extrusion is set within the melting range of this polymer, the extrudate quality becomes very poor, primarily as a result of the crosslinking reaction. Below 320°C, high-quality extrudates are obtained.

As a result of low-temperature deformation in solid-state extrusion, generally, some elastic recovery after the extrusion is expected. For this purpose, we measured the diameter of the extrudates after 1 week room-temperature equilibration. The data are shown in Figure 9. The extrudate swell increases

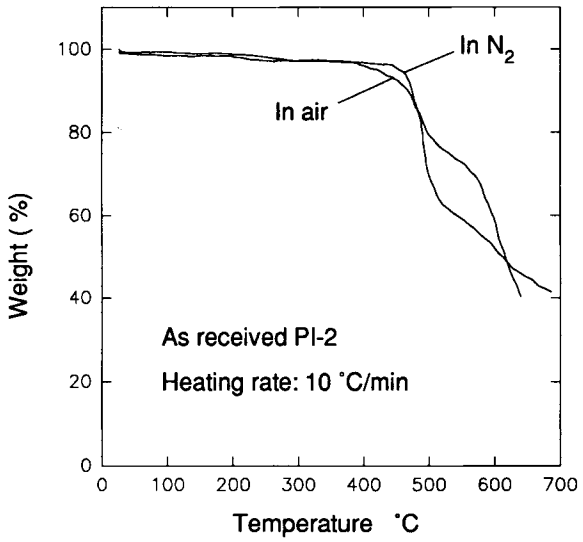

Figure 5 TGA scans of initial BTDA–DMDA in air and dry nitrogen blanket.

with the increase of the extrusion temperature, particularly above 320°C. As observed earlier in the DSC studies, the polymer becomes partially molten and the elastic strains stored during the passage through the die appears to recover quickly before the polymer is completely solidified after it exits the die. This type of behavior has also been observed in the studies by Lee and Cakmak[34,35] and Keller[36] on VF2/VF3 and polyethylenes, respectively. Keller found that there is a dramatic rise in the extrudate swell once the processing temperature reaches the melting-temperature range. This is caused by rapid recovery of the elastically stored deformation after the polymer exits the die. At higher temperatures, it was not possible to measure the extrudate swell because of the melt fracture.

To further investigate the thermal behavior and the mechanism of the solid-state extrusion of the BTDA–DMDA, a series of DSC scans were performed on the extrudates. Figure 10 shows the DSC scans of the extrudates obtained at different temperatures using the largest die with 25.4 mm/min crosshead speed. Here, the die draw ratio is defined as the ratio of the barrel cross-sectional area to the die cross-sectional area:

$$\text{Die draw ratio} = \frac{D^2_{\text{Barrel}}}{D^2_{\text{Die}}}$$

These die draw ratios (DDR) for dies of 4.80, 3.34, and 1.41 mm diameters are 3.94, 8.13, and 45.63, respectively. As the die diameter is decreased, the

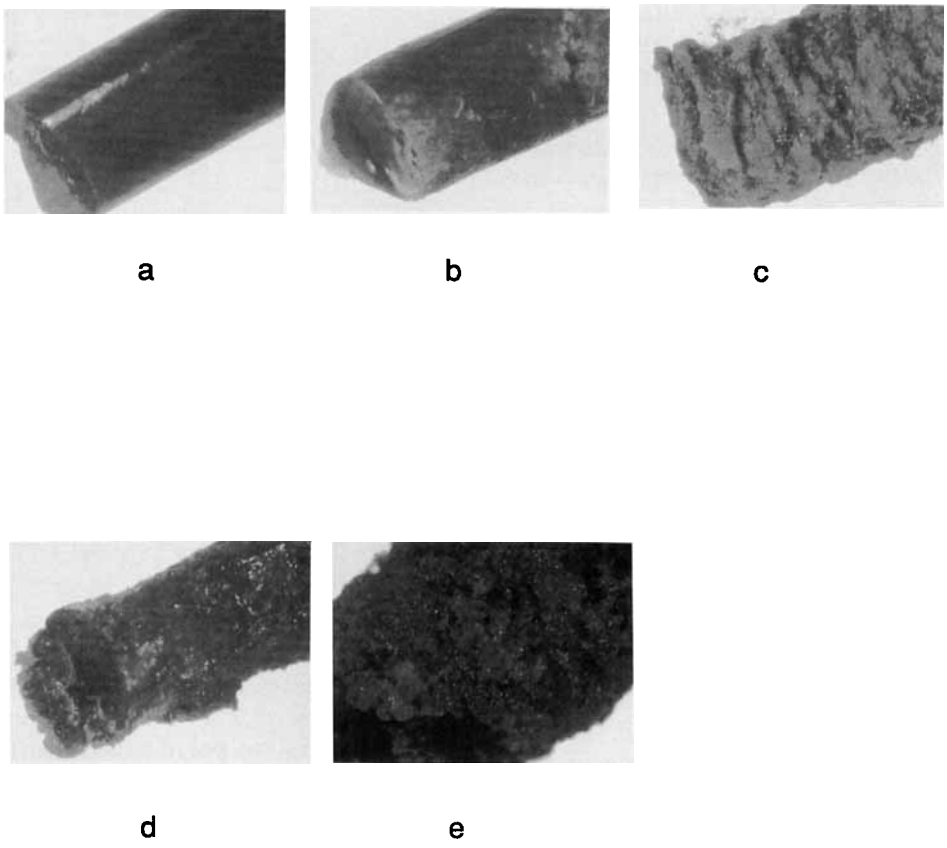

Figure 6 BTDA–DMDA extrudates obtained at different temperatures (Do = 4.80 mm, crosshead speed = 25.4 mm/min): (a) 310°C; (b) 320°C; (c) 335°C; (d) 350°C; (e) 360°C.

deformation that the polymer experiences through the die increases.

The sample extruded at 310°C has no cold crystallization peak. The crystallinity of this sample is fairly high, indicated by the two relatively large melting peaks. The samples extruded at temperatures well within the melting region show cold crystallization peaks after the extrusion process. This cold crystallization peak temperature shifts to higher temperature as the extrusion temperature increases, as shown in both Figures 10 and 11. The areas under these cold crystallization peaks are close to the areas of their corresponding melting peaks, indicating that the extruded BTDA–DMDA remains essentially amorphous. This is rather unusual behavior. At low processing temperatures, the extrudates are highly crystalline, though they appear to have two distinct melting peaks, and at high temperatures, they remain mostly amorphous despite the fact that the extrudates are fairly thick and the core regions experience slower cooling and were expected to exhibit higher crystallinity levels. We did not observe such behavior. The glass transition temperature also increases as the extrusion temperature increases, as shown in Figure 12. The main mechanism that reduces the crystallizability and increases the glass transition temperature at these high extrusion temperature is crosslinking, which is dominant at these temperatures. This crosslinking reaction primarily takes place in the molten phase in the BTDA–DMDA. The higher the extrusion temperature, the higher the reaction rate and the longer time the polymer has to crosslink. The DSC data from the extrudates obtained between 320 and 360°C confirms this. The cold crystallization peaks and the glass transition temperature in the extrudates actually increase with extrusion temperature, indicating that the mobility of the polymer chains are increasingly constrained, resulting in higher temperature crystallization. Extrusion behavior also gives further evidence for the crosslinking: As the extrusion temperature increases, the melt fracture increasingly becomes dominant. Since it is well known that the deformation fields imposed on the polymers in the solid-state extrusion give rise to structural gradients in the radial direction, we first suspected

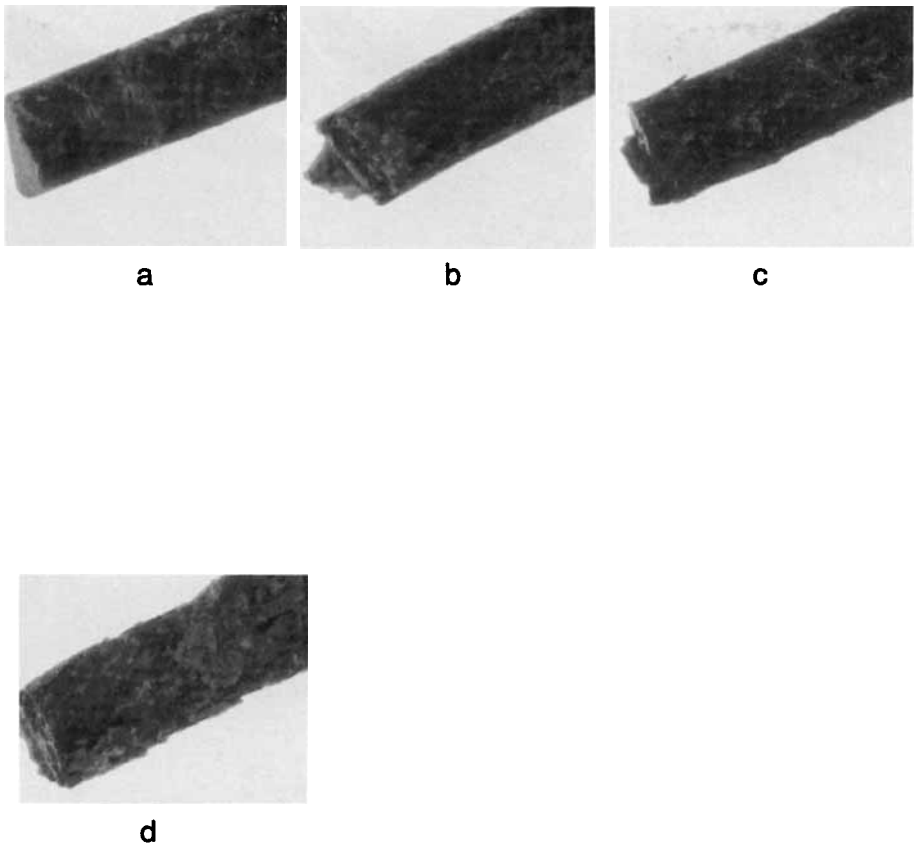

Figure 7 BTDA–DMDA extrudates obtained at different temperatures (Do = 3.34 mm, crosshead speed = 0.381 mm/min): (a) 305°C; (b) 310°C; (c) 315°C; (d) 320°C.

that the dual melting peaks observed in the samples extruded at 310 and 320°C are a result of such a structural gradient. As shown in Figure 13, the DSC scans of three samples obtained at different locations from the surface to the core of the extrudate produced at 310°C show the same DSC traces, indicating the absence of such gradient in this extrudate.

The effects of the die draw ratio and extrusion temperature on the thermal behavior are shown in Figures 14 and 15 for medium- (DDR = 8.13) and small-diameter dies (DDR = 45.6). With these dies, it was not possible to use a 25.4 mm/min extrusion crosshead speed (XHS) and we concentrated on a 0.381 mm/min speed for all extrusion conditions. Figure 14 also indicates dual melting peaks in the sample processed at 305°C; however, the lower-temperature peak area is much larger than that of the higher-temperature peaks. As the extrusion temperature is increased, the areas under the lower-temperature peak decrease and those under the higher-temperature peak increase. The cold crystalization peak also increases in area above the 315°C processing temperature as a result of amorphitization due to the increased levels of crosslinking.

The smallest die (Do = 1.41 mm) imposes the severest deformation on the extrudate (die draw ratio = 45.6). In these extrudates, even at processing temperatures below the melting region, a cold crystallization peak is observed. At such low processing temperatures, we do not think that the crosslinking occurs. The crystallites are destroyed only under the action of the plastic deformation and the proportion of highly oriented but uncrystallized chains increase. Due to their lower entropy, they rapidly crystallize once sufficient thermal energy is provided above the glass transition temperature. But at higher extrusion temperatures, the cold crystallization peak moves to higher temperatures as a result of increased levels of crosslinking. At 315, 320, and 325°C processing temperatures, there appears to be three melting peaks.

From the above investigations, it is quite clear that the extrusion process is practical only at the temperatures below the melting-peak temperature of the BTDA–DMDA material. As shown in Figure 4, the melting-peak temperature is around 327°C. The processing window (305–325°C) of this material is just below this melting-peak temperature. During this solid-state extrusion process, part of the BTDA–

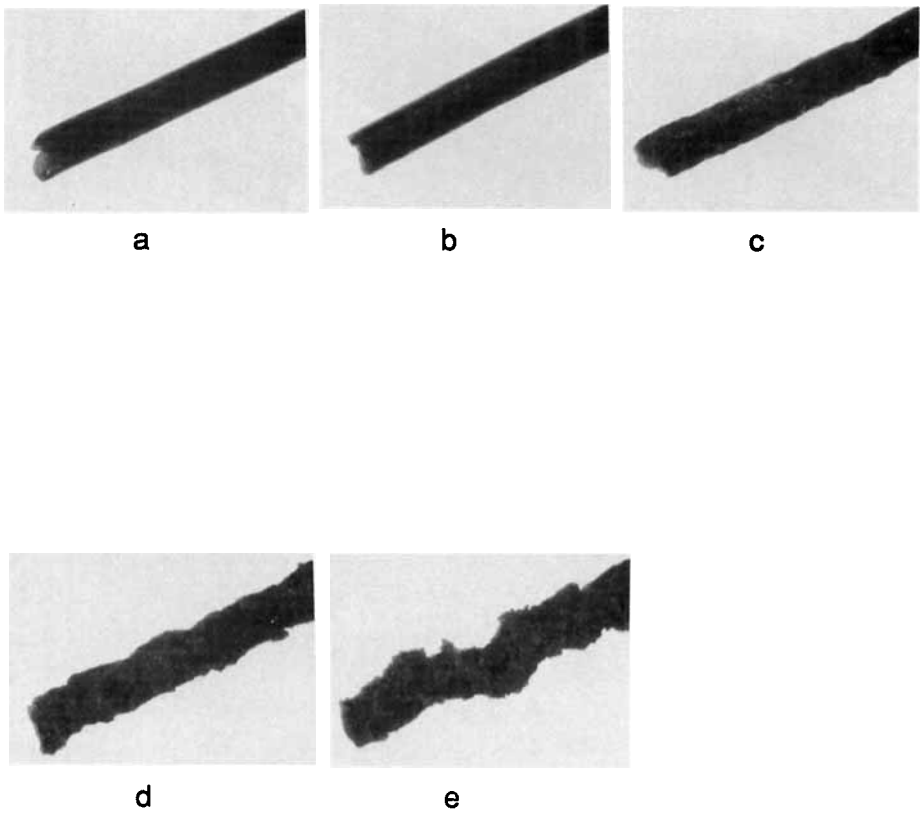

Figure 8 BTDA–DMDA extrudates obtained at different temperatures (*Do* = 1.41 mm, crosshead speed = 0.381 mm/min): (a) 313°C; (b) 315°C; (c) 320°C; (d) 325°C; (e) 330°C.

DMDA crystalline phase melts in the barrel of the rheometer and the melted BTDA–DMDA phase together with the amorphous phase may act as a lubricant, which may ease the flow of the BTDA–DMDA material through the capillary die. When the BTDA–DMDA material flows through the capillary die, it is subjected to a shear stress field which may help the BTDA–DMDA material generate heat to melt the solid crystalline phase. The molten BTDA–DMDA phase may crystallize again into both lower melting crystals and higher melting crystals during the extrusion process.

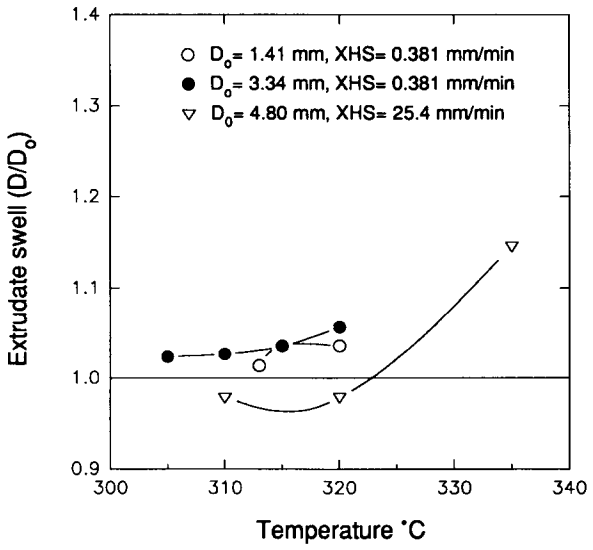

Figure 9 Extrudate swell of BTDA–DMDA with different capillaries.

To verify the origin of the higher melting peak, a series of DSC scans was performed with different heating rates on the extrudate obtained using the largest die (*Do* = 4.8 mm) at 310°C (XHS = 25.4 mm/min). As shown in Figure 16(a), the sample scanned at lower heating rate (5°C/min) shows an exothermic peak between the two large endothermic peaks above the base line, indicating that the material undergoes a recrystallization process during the heating scan. As the heating rate increases, this exothermic peak becomes smaller (at 20°C/min heating rate) and then disappears (at 50°C/min heating rate). Other evidence of this recrystallization process is the change of the relative areas under the two melting peaks. To calculate the areas under the two melting

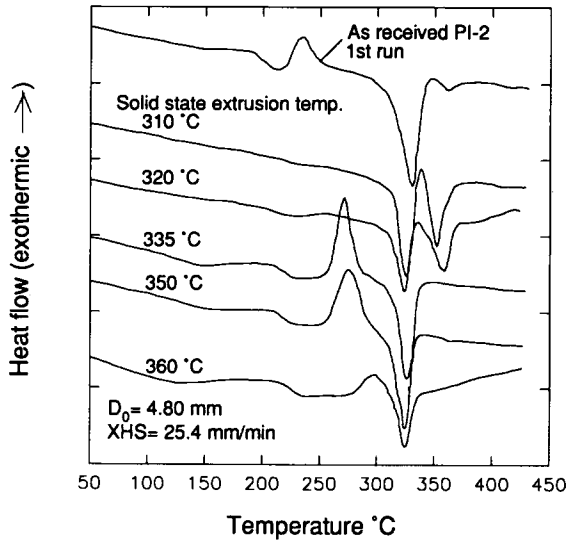

Figure 10 DSC thermograms of BTDA–DMDA extrudates obtained at different temperatures using 4.80 mm-diameter capillary.

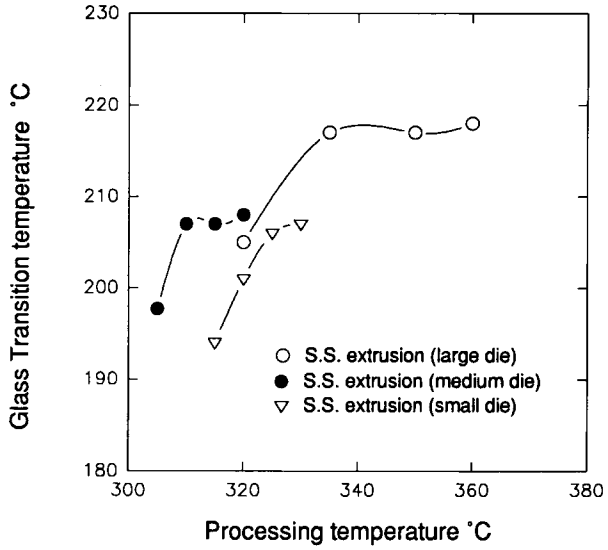

Figure 12 Effect of extrusion temperature on glass transition temperature of BTDA–DMDA extrudates.

peaks for the sample scanned at a 50°C/min heating rate, the two endothermic peaks were separated using a peak separation program. The heat of fusion under the two melting peaks is plotted as a function of the heating rate for the same sample scanned at three different heating rates in Figure 17. At the lower heating rate (5°C/min), the area under the higher melting peak is larger than the one under the lower melting peak. This higher melting peak decreases in its area while the lower melting peak increases as the heating rate increases. The total area under both melting peaks decreases as the heating rate increases.

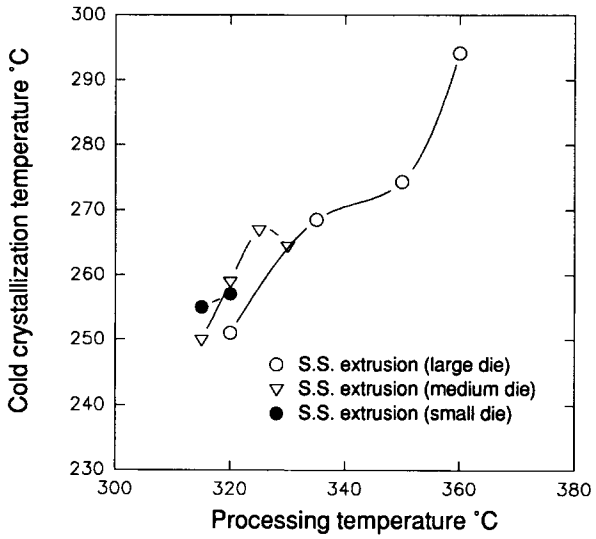

Figure 11 Effect of extrusion temperature on cold crystallization temperatures of BTDA–DMDA extrudates.

All these results indicate that the level of the recrystallization is reduced at a higher heating rate since the material does not have enough time to recrystallize.

This recrystallization process occurs when the lower melting crystals melt. At a lower heating rate, since the level of the recrystallization is higher, the material generates more heat due to the recrystallization process. As a result, the lower melting peak is smaller due to the contribution of the heat from

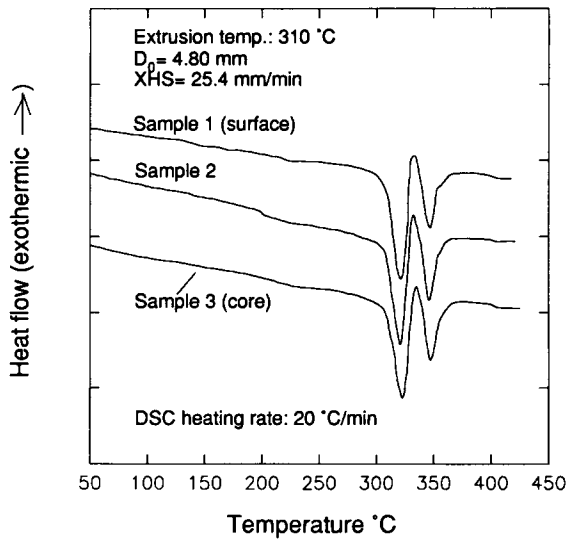

Figure 13 DSC thermograms of three samples obtained at different locations from the surface to the core of the extrudate obtained using 4.80 mm-diameter capillary at 310°C.

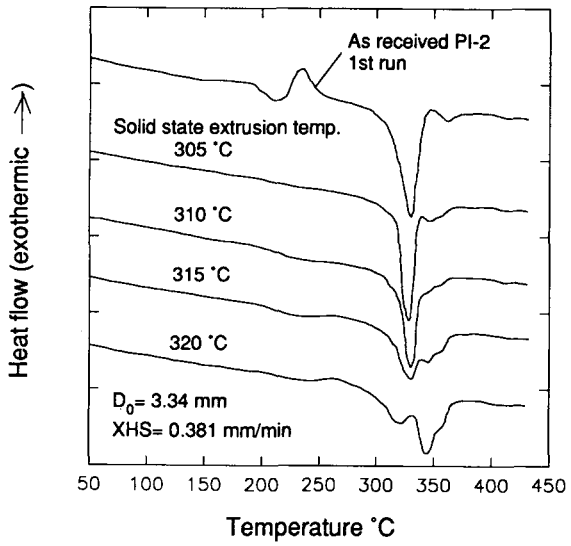

Figure 14 DSC thermograms of BTDA–DMDA extrudates obtained at different temperatures using 3.34 mm-diameter capillary.

the recrystallization process. This recrystallization continues until the higher-temperature crystals melt. It is interesting to note that the sample scanned at 5°C/min shows a third endothermic peak at even higher temperature. This endothermic peak is probably due to the melting of the crystals that previously existed in the sample before the heating process. These preexisted higher melting crystals came with the as-received BTDA–DMDA sample (Fig. 4) and they may have developed during the solid-state extrusion process. Since the DSC heating

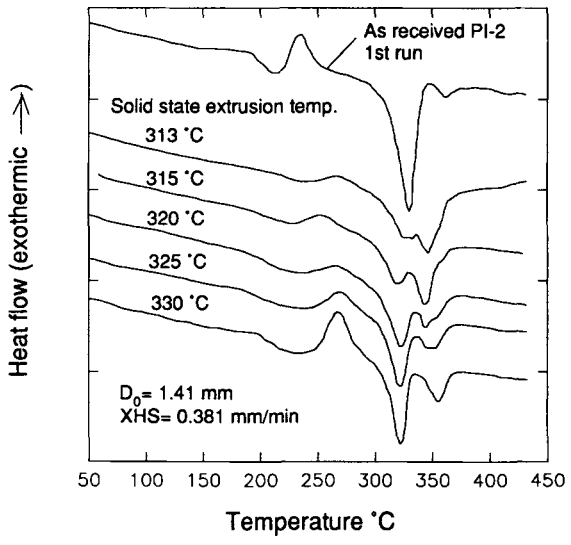

Figure 15 DSC thermograms of BTDA–DMDA extrudates obtained at different temperatures using 1.41 mm-diameter capillary.

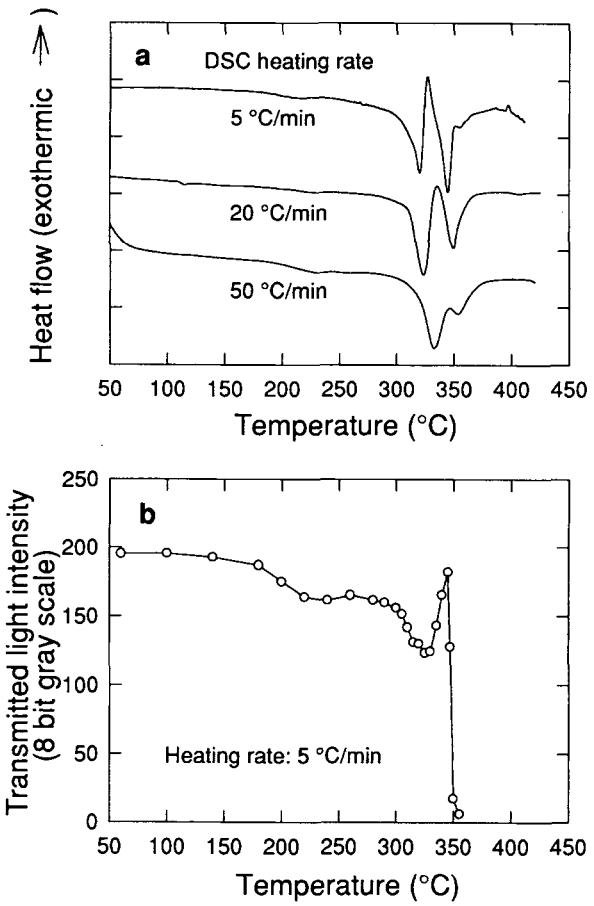

Figure 16 (a) Effect of heating rate on DSC thermograms of BTDA–DMDA extrudate obtained at 310°C using 4.80 mm-diameter capillary. (b) Depolarized transmitted light intensity vs. temperature during the heating scan (5°C/min) for the same sample as in (a).

rate is low, most of the molecules recrystallized at relatively low temperature compared to the higher heating rate sample. As a result, the melting temperature of these recrystallized crystals is slightly lower. This is the reason why we can see the third melting peak. As the heating rate is increased, the melting temperatures of the two peaks shift to the higher temperature due to two reasons: First, the heat of recrystallization is reduced and the recrystallization is completed at relatively higher temperature; the right half of the lower melting peak then becomes more visible, resulting in a slight shift of the lower melting peak to a higher temperature. The recrystallized crystals melt at slightly higher temperature due to the relatively higher recrystallization temperature, resulting in a slight shift of the melting point of the recrystallized crystals. Second, at a higher heating rate, superheating of the sample being

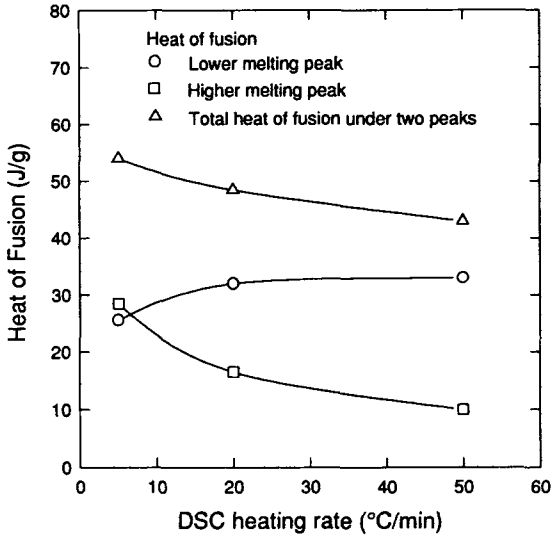

Figure 17 Heat of fusion of BTDA–DMDA extrudate obtained at 310°C using 4.80 mm-diameter capillary.

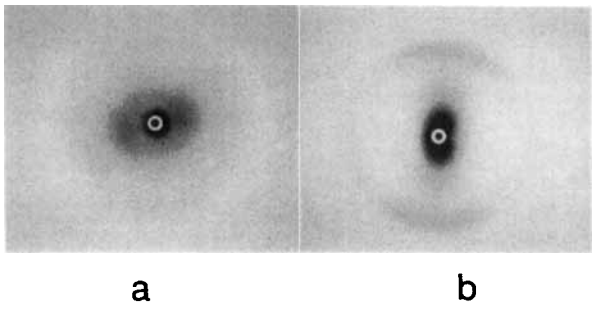

Figure 18 SAXS patterns (extrusion direction vertical) for (a) extrudate obtained using 4.8 mm-diameter capillary at 310°C and (b) extrudate obtained using 1.41 mm-diameter capillary at 315°C.

tested occurs, resulting in the shift of the transitions to higher temperatures.

To further prove the existence of the recrystallization process, a hot-stage video microscopy experiment was performed under cross polarizers on a BTDA–DMDA extrudate processed at 310°C using a 4.8 mm-diameter capillary. As shown in Figure 16(b), the transmitted light intensity decreases with the increase in temperature up to about 230°C and then slightly increases before it decreases again. This slight increase in intensity indicates the cold crystallization process during the heating scan, although the cold crystallization peak is not very obvious on the DSC curve [Fig. 16(a)]. As the temperature is increased further, the transmitted light intensity rapidly decreases, indicating the melting of the lower melting crystals. The molten material is then recrystallized into higher melting crystals, as evidenced by a sharp increase in the depolarized light intensity. These crystals are subsequently melted (the second endothermic peak in the DSC), which causes a rapid decrease in the depolarized light intensity.

In contrast, the sample extruded using the smallest capillary (Do = 1.41 mm) at 315°C does not experience much of the recrystallization process during the DSC heating scan. The higher melting peak (Fig. 15) is due mainly to the melting of the higher melting crystals that preexisted in the sample before the DSC scan. Since the extrusion speed is low for this sample, the material has a longer time to transform its lower melting crystals to higher melting crystals during the extrusion process. Also, if the extrusion temperature and pressure are relatively higher and the deformation is larger, the formation of the higher melting crystals may be favored. As a result, the material crystallizes mainly into higher melting

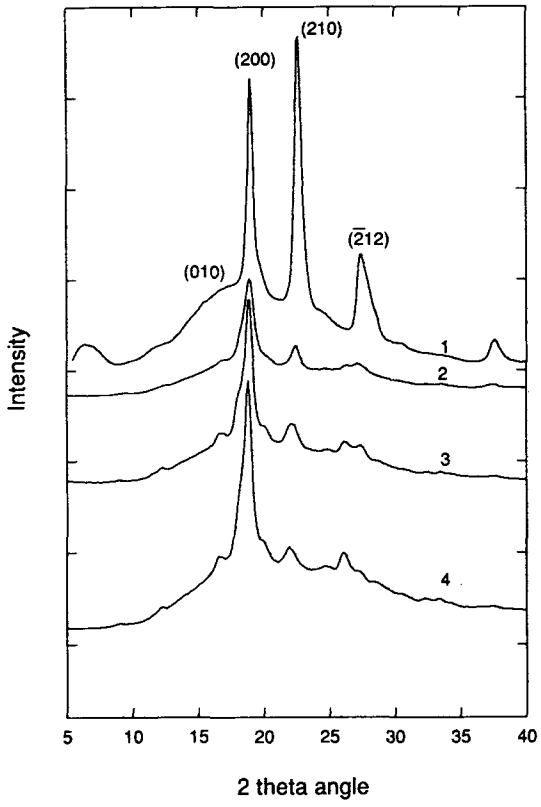

Figure 19 WAXS profiles of BTDA–DMDA samples: (1) compression-molded at 290°C for 10 min; (2) BTDA–DMDA extrudate obtained at 315°C using 1.41 mm-diameter capillary (equatorial scan); (3) annealed BTDA–DMDA extrudate (same sample as #2) at 330°C for 5 min (equatorial scan); (4) annealed BTDA–DMDA extrudate (same sample as #2) at 330°C for 30 min (equatorial scan).

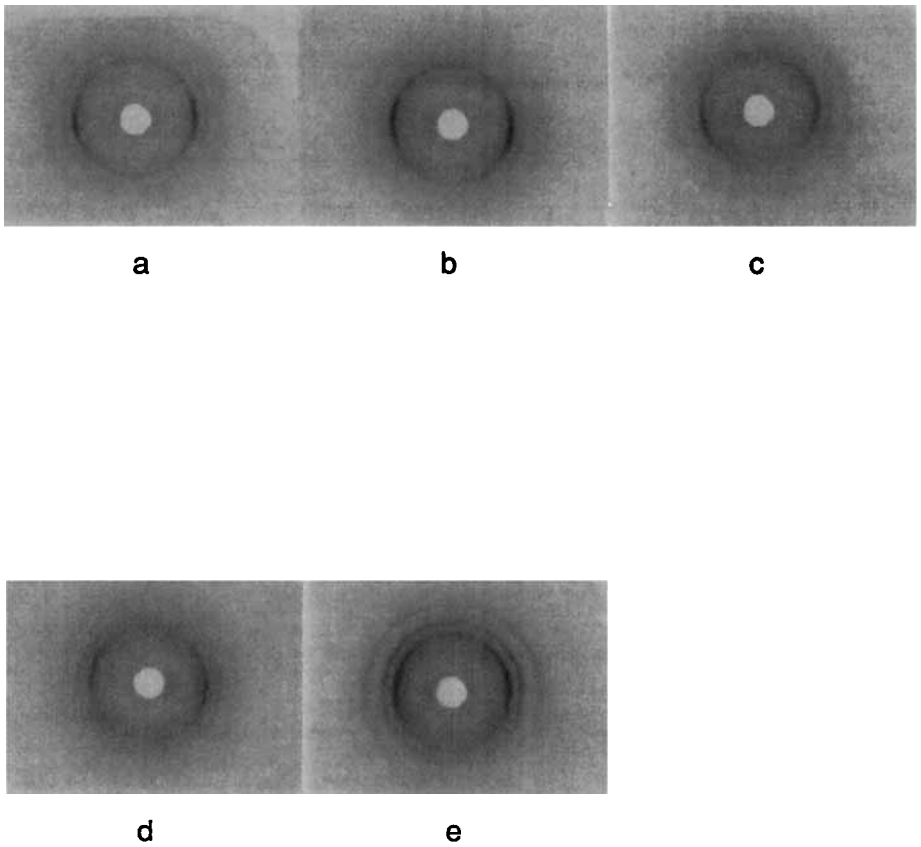

Figure 20 WAXD patterns (extrusion direction vertical) of BTDA–DMDA extrudates obtained at different temperatures using 1.41 mm-diameter capillary: (a) 313°C; (b) 315°C; (c) 320°C; (d) 325°C; (e) 330°C.

crystals during the extrusion process under high pressure.

SAXS Studies on BTDA–DMDA Extrudates

Figure 18 shows SAXS patterns for two samples obtained using capillary dies with the largest diameter (Do = 4.8 mm) (at 310°C) and the smallest diameter (Do = 1.41 mm) (at 315°C), respectively. In both of these patterns, the extrusion direction is vertical. The scattering arc or halo at the largest angle on these two patterns has a d-spacing of 25 Å and it corresponds to the diffraction pattern from the (001) plane of the crystalline structure, which also roughly corresponds to the chain repeat unit length. The sample obtained with the largest die shows a diffuse two-point small-angle scattering maxima with its symmetry axis making about 30° with the equatorial direction. This type of behavior is not unusual for solid-state extruded polymers. Off-meridional symmetry was observed in the solid-state extruded vinylidene fluoride/vinylidene trifluoride (VF2/VF3) copolymers by our group earlier.[34,35] This was attributed to the variations of the orientation across the radial direction. This is primarily caused by the multiple internal yielding and the resulting highly deformed regions exhibit variations in the orientation of the local symmetry axis. What is significant in this sample, however, is that it possesses a higher fraction of the crystalline regions that melt at lower temperature, as observed earlier, and the polymer chains in the crystalline regions partially melt and recrystallize during the DSC heating scan. It should also be pointed out that the two-point pattern is rather diffuse, indicating the considerable disorder in the repeat symmetry in the structure. In contrast, the sample produced using the smallest die shows two-point scattering maxima along the meridional direction with significantly higher intensity and at much smaller angle. The long spacing (172 Å) calculated from the intensity maxima is much larger than that (71 Å) of the sample obtained using the largest diameter cap-

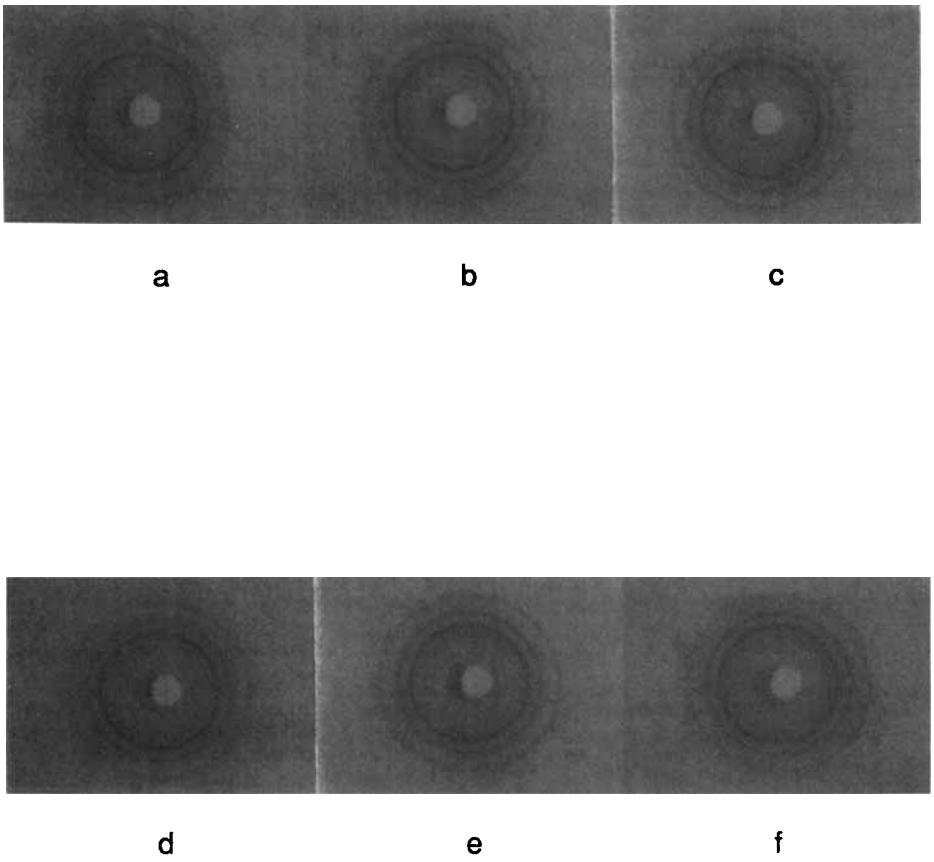

Figure 21 WAXD patterns (extrusion direction vertical) at different locations for the extrudate obtained at 310°C using 4.80 mm-diameter capillary: (a) surface; (b) 0.5 mm from the surface; (c) 1.0 mm from the surface; (d) 1.5 mm from the surface; (e) 2.0 mm from the surface; (f) core.

illary. The latter sample (Do = 1.41 mm, at 315°C) has been observed to contain large-fraction crystallites that melt at higher temperature. This change may also be associated with the change in the crystalline phase as discussed in the WAXD section below.

It has been observed that many polymers show double melting endotherms during their DSC thermal analysis. The origin of such phenomena was attributed mainly to two reasons: First, the double melting peaks may be due to the melting of crystals of two different sizes, each having a different melting temperature. Second, the double melting peaks can also arise from an initial single-peak crystal distribution undergoing melting, recrystallization, and remelting during a DSC upward temperature scan. As we showed above, for BTDA–DMDA extrudates, the existence of the double melting peaks is due to one or both of the two reasons, depending on the processing history that the sample experiences.

WAXS Studies on BTDA–DMDA Extrudate

To study the crystal structure of the BTDA–DMDA extrudate, WAXS profiles were obtained on the sample made from as-received BTDA–DMDA powder by a compression-molding process at 290°C for 10 min under 10 tons of compression force and on the extrudate obtained at 315°C using the small capillary die (Do = 1.41 mm). As indicated in Figure 19, the compression-molded sample shows a WAXS profile very similar to the one obtained by Cheng et al.[1] The peak positions in our samples are close to what they found. This crystal structure reflects the WAXD pattern obtained by the regular crystallization process. However, the extrudate shows a WAXS profile different from the regular profile. There appears a new peak visible at 2θ equal to about 26.2°. There is also a very small shoulder barely visible at 2θ equal to about 18.3°. The diffraction peak at 22.4° is slightly shifted to the lower angle, indicating the possible existence of another

new peak at a slightly lower angle than 22.4°. This evidence may indicate the existence of small amount of a new crystalline phase. As we further annealed the extrudate at 330°C for 5 and 30 min and then quickly quenched them in liquid nitrogen to increase the amount of the higher melting crystals, the diffraction peak at 27.2° decreases while the new peak at 26.2° increases, the shoulder at about 18.3° becomes more visible, and the formation of another new peak at 21.9° is visible. This experiment proves the formation of a new crystalline phase during the solid-state extrusion process and also during the DSC upward temperature scan. Through the peak separation process, the positions of the new peaks are identified and they are listed in Table I.

The existence of the new crystalline phase has also been proven by Chalmers et al.[2] on their compression-molded and annealed samples. Through their WAXD studies, they found a new crystalline phase with a new diffraction peak at $2\theta = 18°$.

As shown in Figures 4 and 10, quenched BTDA–DMDA from the melt and extruded BTDA–DMDA at temperatures higher than its lower melting temperature are in an amorphous state. These samples usually crystallize into the lower melting crystals during their DSC heating scan. However, the solid-state extruded samples usually exhibit two melting peaks. This difference can be explained as follows:

In the solid-state extrusion process at temperatures between 300 and 330°C, the material crystallizes into two different crystalline phases under high pressure. The relative content of each phase depends on the extrusion pressure and temperature. The formation of the higher melting crystals is favored at high pressure and at relatively high temperature. In the case of the extrudate obtained using the largest capillary (Do = 4.8 mm) at 310°C, the majority of the crystallizable molecular chains are packed into the lower melting crystals while the higher melting crystalline phase is also developed although its content is low. Upon further heating of this sample, the lower melting crystals melt first, and the higher melting crystalline phase further develops. Since the molecules are highly packed by the solid-state extrusion process, once they are released from the lower melting crystals, they have a good conformational rearrangement and they are ready to grow on the preexisting higher melting crystals. This higher-melting phase then melts as the temperature is further increased. In comparison, the extrudate produced using the smallest capillary (Do = 1.41 mm) at 315°C possesses a higher content of the higher melting crystals. The appearance of the large higher melting peak is thus expected. In contrast to the solid-state extrusion, the regular crystallization process usually produces only lower melting crystals, as we observed from the DSC scans of the amorphous BTDA–DMDA samples.

Table I WAXD Peaks (2θ) for BTDA–DMDA

Observable 2θ for Regular Crystallized BTDA–DMDA	New Peaks 2θ
16.74	8.97
18.82	12.19
22.39	18.30
27.27	21.87
37.53	26.17

Microbeam X-ray Diffraction Studies on BTDA–DMDA Extrudates

To study the effect of extrusion temperature on the orientation level of the BTDA–DMDA extrudates, a series of WAXD pictures were taken using the microbeam X-ray diffraction technique on the extrudates obtained using the small die at different temperatures. The diffraction patterns shown in Figure 20 indicate that all the samples obtained at different temperatures possess about same degree of orientation. The molecules tend to be oriented in the extrusion direction. The effect of the extrusion temperature on the orientation development of the extrudates is not very significant.

To investigate the orientation gradient developed during the solid-state extrusion process, several WAXD patterns were taken from the surface to the core along the radial direction on the extrudate obtained using the largest die at 310°C. These patterns show that the molecules are almost randomly oriented (Fig. 21). No preferential orientation was found at several different locations from the surface to the core. It is clear from the above studies that a small diameter capillary induces a higher molecular orientation level in the extrudate compared to the larger diameter capillary as a result of increased deformation during the process.

CONCLUSIONS

It is possible to extrude the BTDA–DMDA below its melting peak temperature. High-quality extrudates were obtained at temperatures between 305 and 325°C. Above the melting-peak temperature, the

extrudates showed degradation and melt fracture as a result of crosslinking.

The BTDA–DMDA samples obtained at lower processing temperatures generally showed two distinct endothermic peaks in their DSC scans. The higher endothermic peak is due to the melting of the new crystalline phase developed partially through the solid-state extrusion process and partially through the recrystallization process during the DSC heating scan. This was confirmed with DSC, depolarized light hot-stage video microscopy, and WAXD studies.

The effect of extrusion temperature on the orientation level of the BTDA–DMDA extrudates was found to be rather small. The extrudates that have undergone a larger deformation during the extrusion through the smaller dies exhibit higher chain orientation along the extrusion direction. However, the degree of orientation obtained in these extrudates are unusually low. Also, the orientation does not vary significantly in the radial direction, as evidenced by the microbeam X-ray measurements.

Funding for this research was partly provided by M. C.'s NSF Presidential Young Investigator Grant # DDM-8858303.

REFERENCES

1. S. Z. D. Cheng, M. L. Mittleman, J. J. Janimak, D Shen, T. M. Chamlers, H. S. Lien, C. C. Tso, P. A. Gabori, and F. W. Harris, *Polym. Int.*, **29,** 201 (1992).
2. T. M. Chalmers, A. Zhang, D. Shen, S. H. S. Lien, C. C. Tso, P. A. Gabori, F. W. Harris, and S. Z. D. Cheng, *Polym. Int.*, **31,** 261 (1993).
3. J. H. Southern and R. S. Porter, *Chem. Eng. News Am. Chem. Soc.*, **Sept. 22,** 45 (1969).
4. J. H. Southern and R. S. Porter, *J. Macromol. Sci. Phys. B,* **4,** 541 (1970).
5. J. H. Southern and R. S. Porter, *J. Appl. Polym. Sci.*, **14,** 2305 (1970).
6. K. Imada, T. Yamamoto, K. Shigomatsu, and M. Takayanagi, *J. Mater. Sci.*, **6,** 537 (1971).
7. K. Imada and M. Takayanagi, *Int. J. Polym. Mater.*, **2,** 89 (1973).
8. P. Predecki and W. O. Statton, *J. Polym. Sci. B,* **10,** 87 (1972).
9. T. Niikuni and R. S. Porter, *J. Mater. Sci.*, **9,** 389 (1974).
10. A. G. Gibson, I. M. Ward, B. N. Cole, and B. Parsons, *J. Mater. Sci.*, **9,** 1193 (1974).
11. K. Nakayama and H. Kanetsuna, *J. Mater. Sci.*, **10,** 1105 (1975).
12. C. L. Lee, R. M. Caddell, and G. S. Y. Yeh, *Mater. Sci. Eng.*, **10,** 241 (1972).
13. J. H. Southern, N. E. Weeks, R. S. Porter, and R. G. Crystal, *Makromol. Chem.*, **162,** 19 (1972).
14. N. E. Weeks, S. Mori, and R. S. Porter, *J. Polym. Sci. Polym. Phys. Ed.*, **13,** 2031 (1975).
15. S. M. Aharoni and J. P. Sibilia, *J. Appl. Polym. Sci.*, **23,** 133 (1979).
16. M. Ito, J. R. C. Pereira, S. L. Hsu, and R. S. Porter, *J. Polym. Sci. Polym. Phys. Ed.*, **21,** 389 (1983).
17. B. S. Kim and R. S. Porter, *J. Polym. Sci. Polym. Phys. Ed.*, **26,** 2499 (1988).
18. A. E. Zachariades, P. D. Griswold, and R. S. Porter, *Polym. Sci. Eng.*, **19,** 441 (1979).
19. S. J. Pan, H. R. Brown, A. Hiltner, and E. Baer, *Polym. Eng. Sci.*, **26,** 997 (1986).
20. S. J. Pan, H. I. Tang, A. Hiltner, and E. Baer, *Polym. Eng. Sci.*, **27,** 869 (1987).
21. H. I. Tang, A. Hiltner, and E. Baer, *Polym. Eng. Sci.*, **27,** 876 (1987).
22. N. J. Capiati, S. Kojima, W. Perkins, and R. S. Porter, *J. Mater. Sci.*, **12,** 334 (1977).
23. K. Nakamura, K. Imada, and M. Takayanagi, *Int. J. Polym. Mater.*, **2,** 71 (1972).
24. A. Buckley and H. A. Long, *Polym. Eng. Sci.*, **9,** 115 (1969).
25. N. G. McCrum, B. E. Read, and G. Williams, *Anelastic and Dielectric Effects in Polymer Solids,* Wiley, London, 1967, p. 353.
26. C. S. Lee, R. M. Caddell, and G. S. Y. Yeh, *Mater. Sci. Eng.*, **241,** 10 (1972).
27. J. B. Enns and R. Simha, *J. Macromol. Sci.-Phys. B,* **13,** 11 (1977).
28. J. P. Sibilia, R. J. Schaffhauser, and L. G. Roldan, *J. Polym. Sci. Polym. Phys. Ed.*, **14,** 1021 (1976).
29. A. Ya. Goldman, A. N. Grinman, and Yu. F. Dunichev, *Polym. Mech.*, **11,** 340 (1975).
30. A. Buckley and H. A. Long, *Polym. Eng. Sci.*, **9,** 115 (1969).
31. C. S. Lee, R. M. Caddell, and G. S. Y. Yeh, *Mater. Sci. Eng.*, **241,** 10 (1972).
32. S. M. Aharoni and J. P. Sibilia, *Polym. Eng. Sci.*, **19,** 450 (1979).
33. J. H. Southern, N. J. Capiati, T. Kanamoto, R. S. Porter, and A. E. Zachariades, Eds., *Encyclopedia of Polymer Science and Engineering,* 2nd ed., Wiley, New York, 1989, Vol. 15, p. 346.
34. J. S. Lee and M. Cakmak, *Polym. Eng. Sci.*, **33,** 1559 (1993).
35. J. S. Lee and M. Cakmak, *Polym. Eng. Sci.*, **33,** 1570 (1993).
36. A. Keller, private communication.

Received August 5, 1994
Accepted November 13, 1994